Science of the Total Environment 957 (2024) 177638

Contents lists available at ScienceDirect

Science of the Total Environment

journal homepage: www.elsevier.com/locate/scitotenv

Hot spot volcano emissions as a source of natural iron fertilization in the ocean

David González-Santana [a,*], Melchor González-Dávila [a], Aridane G. González [a], Alfonso Medina-Escuela [b], David Fariña [b], J. Magdalena Santana-Casiano [a]

[a] Instituto de Oceanografía y Cambio Global, IOCAG, Universidad de Las Palmas de Gran Canaria, ULPGC, Spain
[b] Institute for Applied Microelectronics (IUMA), Universidad de Las Palmas de Gran Canaria, Campus de Tafira, 35017 Las Palmas de Gran Canaria, Spain

HIGHLIGHTS

- Coastal volcanoes are local Fe sources, through molten lava and ash deposition.
- ~99 % of the iron was found in the particulate phase.
- Soluble Fe concentrations were ~10 times higher than generally found in open Atlantic Ocean waters.
- Particulate Fe rapidly sinks, however, solubilisation acts as a long-term source.

GRAPHICAL ABSTRACT

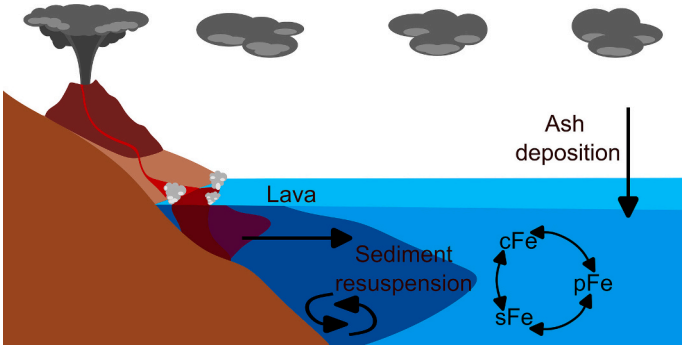

ARTICLE INFO

Editor: Julian Blasco

Keywords:
Iron
Fertilization
Volcano
Ash
Molten lava
Seawater

ABSTRACT

Dust deposition, river runoff and glacial melt are the main sources of trace metals to the surface ocean. In the Canary Islands, deposition is dominated by dry dust deposition from the Saharan desert. However, during 85 days, from 19 September to 13 December 2021, the main source of trace metals on the island of La Palma changed drastically. The eruption of the Tajogaite volcano released tonnes of volcanic ash. Concurrently, several lava flows reached the coastal waters. Volcanic activity on land became the main source of iron (Fe) into the coastal waters. Fe concentrations in seawater reached over 1900 nmol L^{-1}. ~99 % of the iron was found in the particulate phase (particles >0.2 μm wide; 1920 ± 50 nmol L^{-1}). Colloids, smaller size particles (0.02 μm < colloids < 0.2 μm) represented ~0.7 % of the iron pool (14.5 ± 0.5 nmol L^{-1}). While the truly soluble phase represented ~0.03 %. However, the soluble phase presented concentrations reaching 0.66 ± 0.05 nmol L^{-1}, which is ~10 times higher than generally found in open Atlantic Ocean waters. The results show how the Fe size fractionation evolved during the eruption, from a dominance of large particle phases to smaller-sized compounds.

* Corresponding author.
E-mail addresses: david.gonzalez@fpct.ulpgc.es (D. González-Santana), melchor.gonzalez@ulpgc.es (M. González-Dávila), aridane.gonzalez@ulpgc.es (A.G. González), aescuela@iuma.ulpgc.es (A. Medina-Escuela), dfarina@iuma.ulpgc.es (D. Fariña), magdalena.santana@ulpgc.es (J.M. Santana-Casiano).

https://doi.org/10.1016/j.scitotenv.2024.177638
Received 26 September 2024; Received in revised form 14 November 2024; Accepted 17 November 2024
Available online 26 November 2024

1. Introduction

The arrival of lava in the ocean from a single large eruption can have a significant impact on the surface iron (Fe) budget, potentially increasing Fe concentrations by tens or hundreds of nanomoles per litre of seawater (Olgun et al., 2011). The main ways in which a subaerial volcanic eruption can become a source of Fe to the ocean are direct mobilisation from dry ash deposited in seawater (dry deposition), mobilisation from ash through interaction with cloud water before entering surface seawater as rain (wet deposition), and interaction of molten lava with seawater through hydrothermal processes (Duggen et al., 2007, 2010; Olgun et al., 2011; Sansone and Resing, 1995).

Volcanic tephra presents a wide range of sizes. Volcanic ash is composed of a mixture of particles <2 mm in diameter such as glass shards (quenched magma fragments), pyrogenic minerals (i.e. silicates and oxides) and lithic particles (e.g. eroded rock material from the volcanic conduit of any origin (Frogner et al., 2001)). These components can potentially release Fe on different time scales when in contact with seawater (Fisher and Schmincke, 1984; Óskarsson, 1981).

The importance of volcanic ash (dry or wet deposition) as a source of Fe is poorly characterised compared to aeolian or desert mineral dust. Dust is known to be an important atmospheric source for the biogeochemical Fe cycle in the surface ocean (Breitbarth et al., 2010; Olgun et al., 2011; Tagliabue et al., 2017). The hypothesis that volcanic ash can release bioavailable Fe into the ocean in the same way as dust was established in the early 1990s (Spirakis, 1991). The first experiment with volcanic ash to assess the solubility of Fe and phytoplankton-relevant nutrients in seawater was carried out with ash from the 1991 eruption of Hekla, Iceland (Frogner et al., 2001). Since then, geochemical experiments with volcanic ash from both subduction zone and hot spot volcanoes (Olgun et al., 2011) have shown a significant release of Fe when pristine volcanic ash meets seawater. At seawater pH, the calculated global mean of Fe released from volcanic ash is 200 ± 50 nmol Fe/g ash. This release is comparable to the calculated range for desert dust of 10–125 nmol Fe/g dust (Olgun et al., 2011; Spokes and Jickells, 1996).

Current estimates indicate that 3.91 (2.45–6.59) $\times 10^{13}$ kg of ash and pyroclasts were formed between 1980 and 2019 (Galetto et al., 2023). Material deposited on land forms soils that are highly fertile (El-Desoky et al., 2018). Similarly, recent articles have shown that ash deposition can lead to phytoplankton blooms in the surface ocean (Kelly et al., 2023; Rogan et al., 2016; Wilson et al., 2019). However, ash deposition in both environments leads to different outcomes. On land, ash deposition generally results in soil formation. However, ash and pyroclastic deposition in the ocean is generally followed by precipitation due to density differences between seawater and the volcanic material. It is therefore important to consider what happens to the tonnes of ash that reach the surface ocean each year, and what happens to the iron contained in this volcanic material.

When volcanic ash is exposed to seawater, Fe can be dissolved by two mechanisms: dissolution of iron-bearing salt coatings on the surface of ash particles, or dissolution of silicate glass and silicate and non-silicate mineral components of the ash (glass shards, crystalline igneous and non-igneous minerals, secondary minerals formed by hydrothermal processes) (Frogner et al., 2001; Maters et al., 2016). It thus becomes bioavailable Fe. An important factor is the rapid release (minutes to hours) of Fe from the ash, which is dominated by the rapid dissolution of surface salts rather than the glass shards (Duggen et al., 2007, 2010; Olgun et al., 2011). Laboratory experiments with hot spot volcanic ash (HSVA) from different sites have shown that between 35 and 107 nmol Fe/g ash are released within the first 60 min of contact with seawater. Subduction zone volcanic ash (SZVA) releases a higher concentration, between 35 and 340 nmol Fe/g ash. However, the alteration of volcanic ash particles deposited as an ash layer on the seafloor on a longer time scale (days to weeks to years) is controlled by their bulk chemical composition. It has been hypothesised that large-scale Fe fertilization by volcanic ash may have longer-term effects on the order of thousands of years through changes in the ratio of inorganic to organic carbon rainfall associated with a diatom phytoplankton bloom (Watson, 1997).

The total Fe content in the volcanic ash and the volcanic glass shards (quenched magma fragments) can vary from 1 to 11 wt% (Olgun et al., 2011). In comparison, desert dust samples, for example, those from Cape Verde, have a 6.5 wt% concentration (Olgun et al., 2011). The total Fe content of volcanic ash samples ranges from 1.2 to 8.0 wt%. Ash particles (tephra <2 mm in size) are coated with a thin layer of salts in the form of Fe sulphates and Fe halides formed by the interaction of ash particles with volcanic gases (S, HCl and HF) and aerosols in the eruption plume (Delmelle et al., 2007; Naughton et al., 1976). Glass compositions, based on total alkali versus silica content, range from andesitic to rhyolitic (SZVA) and from basaltic to andesitic (HSVA). The Fe content of the volcanic glass shards ranges from 1 to 11 wt%, with significantly lower values for SZVA compared to HSVA samples (Olgun et al., 2011). The Fe content of pyrogenic minerals ranges from traces in plagioclase to 10–30 wt% FeO in clinopyroxene and up to 50–70 wt% in magnetite (Nakagawa and Ohba, 2002).

On the other hand, the interaction between the molten lava and seawater produces a variety of reactions that act as sources of Fe and other elements and also change the chemical composition of the surrounding seawater (De Ronde et al., 2007a; González-Delgado et al., 2021; González-Santana et al., 2022; Mason et al., 2021). Degassing and solidification reactions occur before lava from a volcano reaches the coast and reacts with seawater. They depend on the time taken by the lava flows to travel from the source area (De Ronde et al., 2007b; Gíslason et al., 2002; Olafsson, 1975; Resing and Sansone, 1999, 2002; Sansone and Resing, 1995). The release of metals during lava-sea interaction occurs through three processes: 1) bulk dissolution of elements into seawater in proportion to their abundance in basalt, 2) additional release of chalcophile elements during degassing of the cooling lava, and 3) precipitation of insoluble elements and subsequent scavenging of "particle-reactive" elements (Hawco et al., 2020; Resing and Sansone, 2002).

This manuscript aims to present the iron size speciation within the coastal environment during an active subaerial volcano eruption in La Palma island (Canary Islands, Spain) in 2021. It is important to remark that the arrival of lava to the ocean was not homogeneous, there were moments were incandescent lava and laze formation was visible, followed by cooling down periods. Moreover, sampling started before the arrival to the ocean and continued after the end of the eruptive phase.

2. Materials and methods

2.1. Study site

The study area was based on the Tajogaite volcano-affected coastal region of La Palma Island. The affected area was characterised by the presence of an 80 to 110 m cliff in the northern section and volcanic black sandy beaches in the central and southern sections. The REDMIC (2022) shows that the subsurface area presented a soft slope (3°). The 25 m isobath was found 500 m from the shoreline. The 50 m isobath was located 650 to 750 m (northern and southern sections, respectively) from the shoreline. The northern section is characterised by the presence of several deep canyons.

Lava reached the coastal waters of Tazacorte in three different places at different times during the 85 days of volcanic activity. The eruption started on 19 September and reached the coast on 28 September, 10 November and 22 November. Sampling stations were moved according to their distance from the coast at the time of sampling. Stations sampled before 28 September are currently covered by lava.

2.2. Sampling

Surface iron samples were collected during 13 visits to the

volcanically affected coastal area of Tazacorte (La Palma, Spain; Fig. 1, Table 1). A detailed description of the sampling for physico-chemical parameters, including the CO_2 system, has already been published by González-Santana et al. (2022). Surface waters near the lava delta in the coastal waters were collected on board three vessels based on availability during the sampling days, the Salvamar Alphard and Pico Teide made of fiber and rubber, and a rubber dinghy operated by the Spanish Guardia Civil.

Oceanographic parameters such as depth, temperature, salinity (conductivity), chlorophyll-*a*, turbidity, dissolved oxygen (DO) and pH were measured using AAQ-Rinko™ (JFE Advantech Co. Hyogo, Japan) water profiler which recorded every 0.1 s. The DO sensor was calibrated daily and compared with discrete samples analysed by the Winkler method (modified by Strickland and Parsons, 1972) using an automated titration system with potentiometric endpoint detection (Titrino 848, Metrohm™, Metrohm AG, Herisau Switzerland). A TRIS artificial seawater standard (Millero, 1986) was prepared for pH. Replicate measurements (average n = 7 for the different study days) of the TRIS buffer standard were better than ±0.003 pH units with accuracy against the theoretical TRIS buffer value of ±0.006 units. The pH sensor was calibrated daily in total scale and measured under in-situ seawater temperature and salinity conditions, $pH_{T,is}$. These results have been reported in a previous publication (González-Santana et al., 2022).

Iron samples were collected in 1 L low-density polyethylene (LDPE) acid-cleaned bottles (Cutter et al., 2017). Subsamples were collected on shore inside a bubble laboratory. Unfiltered 60 mL subsamples were collected for total dissolvable iron (TdFe). The dissolved iron (dFe) samples were filtered through a 0.2 μm pore size filter (Sartorius PES). The soluble iron (sFe) samples were first filtered using the same procedure as the dFe sample, and then filtered through a 0.02 μm syringe

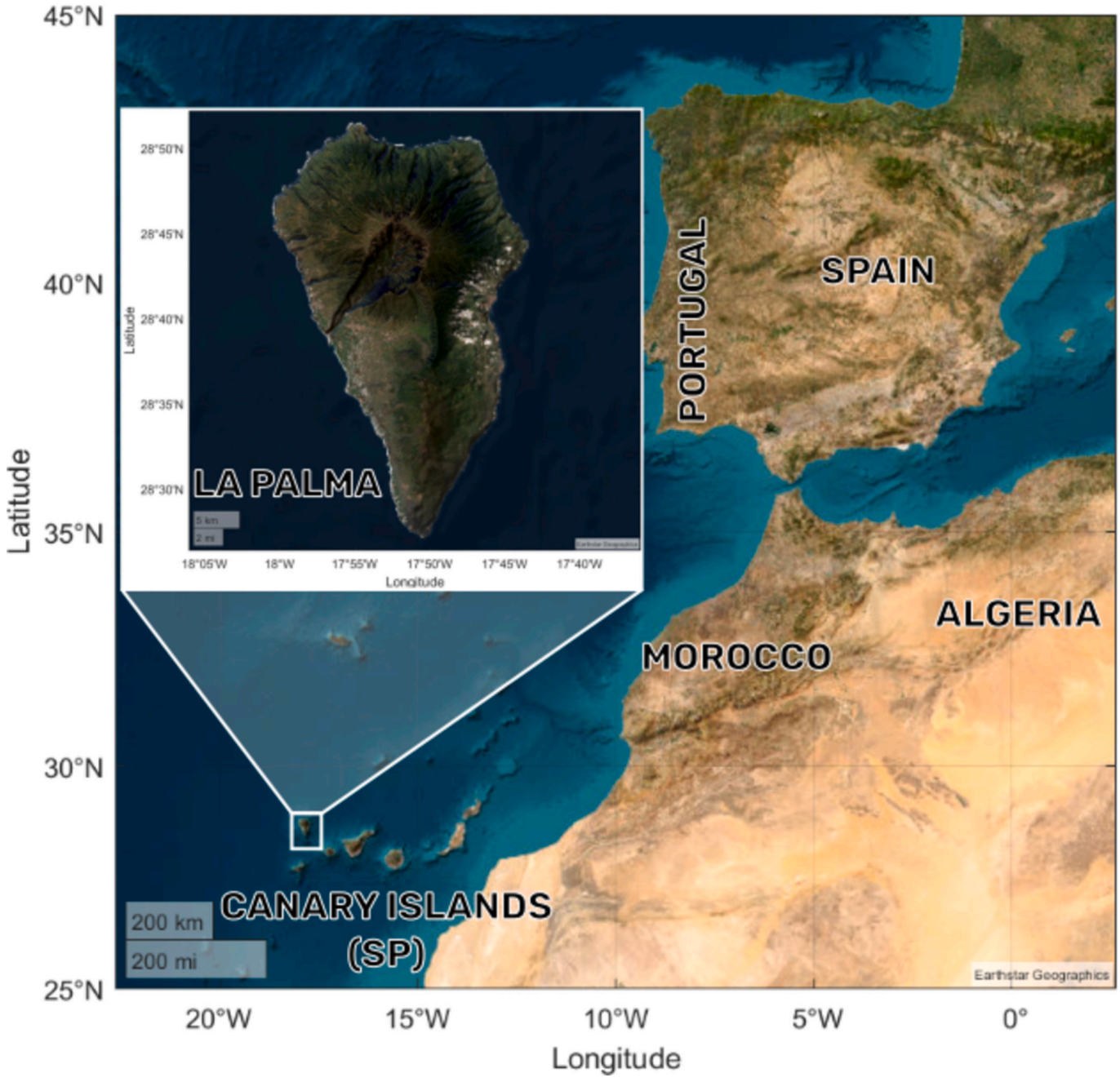

Fig. 1. La Palma island is one of the eight islands forming the Canarian Archipelago, which is part of Spain. The Canary Islands are about 1100 km Southwest of mainland Spain.

Table 1
Sampling dates and the seawater chemical characteristics (sea surface temperature, SST in °C; sea surface salinity, SSS; in situ pH in Total scale, $pH_{T,is}$; and dissolved oxygen concentration, DO in μmol kg^{-1}).

Date	SST	SSS	$pH_{T,is}$	DO
09-22-21	25.15	37.17	7.990	217.4
09-23-21	24.56	36.87	7.965	223.8
09-30-21	37.00	37.18	7.581	168.3
10-01-21	30.80	37.15	7.795	188.7
10-02-21	24.91	36.90	7.938	202.8
10-08-21	26.91	36.93	7.901	203.3
10-23-21	23.98	37.08	7.952	212.6
11-08-21	23.60	36.94	7.985	212.3
11-12-21	46.33	37.69	7.017	134.8
11-14-21	30.02	37.09	7.912	192.4
11-20-21	29.08	36.94	7.864	191.1
12-08-21	22.39	36.99	7.946	215.3
01-11-22	21.48	37.11	8.012	221.4

filter (Whatman® Anotop®) using a peristaltic pump at a rate of 1 mL min^{-1}. All samples were acidified to 2 ‰ v/v (pH ~1.7; final concentration of 0.024 M HCl) using ultrapure HCl (Sigma-Aldrich). Samples were stored in the dark for at least 6 months before analysis.

2.3. Iron concentration analysis

The TdFe, dFe and sFe samples were analysed in duplicate (two analytical peaks; a second duplicate was performed if the standard deviation was >5 %) using flow injection analysis with chemiluminescence detection (Bruland and Lohan, 2006; Obata et al., 1993) in an ISO Class-5 laminar flow hood inside an ISO Class-6 clean laboratory. Sample concentrations are given as "average" ± "standard deviation of the analysis". If an average of samples is calculated, the weighted average ± the combined standard deviation is used.

Samples were spiked with 0.013 M ultrapure H_2O_2 (Sigma-Aldrich) 30 min before analysis to ensure complete oxidation of Fe(II) to Fe(III) (Lohan et al., 2006). Each sample was buffered in-line to pH 3.5 to 4.0 using 0.15 M ammonium acetate (Supelco and Sigma-Aldrich) before the Fe was preconcentrated on a Toyopearl AF-Chelate 650 M cation exchange resin (Tosohaas) between 30 and 120 s at a flow rate of 1.5 mL min^{-1}. After a rinsing step with a weak 0.013 M HCl (Sigma-Aldrich), Fe was released from the resin with 0.24 M HCl (Sigma-Aldrich) and introduced into the reaction stream, where it was mixed with a 0.015 mM luminol solution containing 70 μL L^{-1} triethylenetetramine (Sigma-Aldrich), buffered to pH 9.5 ± 0.1 with a 1 M ammonia solution (Supelco). Iron concentrations were quantified by performing a 10-point calibration curve (TraceCERT) using low-Fe seawater. The calibration curve range varied by Fe concentrations, where samples with high Fe concentrations were reanalysed in a wider range calibration curve. The limit of detection (three times the standard deviation of the lowest addition of the lowest calibration curve of up to 1 nM) was 0.03 ± 0.02 nM, while the precision of three analytical peaks was <2 %. Accuracy was established by repeat measurements of an in-house standard.

The in-house standard was collected at the European Time-Series Station in the Canary Islands (ESTOC; 29° 10′ N 15° 30′ W) within the oligotrophic North Atlantic subtropical gyre. The seawater was collected at 20 m depth using a trace metal clean Teflon pump (PFD2 316F, AstiPure®) and filtered by 0.2 μm dual pore-size trace metal clean filters (Acropack™). The in-house standard was characterised by a ICP-MS Element XR instrument (Thermo Fisher, Bremen, Germany) coupled with an online seaFAST system (Elemental Scientific™), at Pôle Spectrométrie Océan (IFREMER, France), which used GSC as the reference sample (1.59 ± 0.04 nM, in agreement with the reported consensus values, 1.54 ± 0.12 nM).

3. Results and discussion

On 19 September 2021, after a very short period of intense and continuous seismic activity in the area, the Tajogaite volcano (Cumbre Vieja Ridge, La Palma, Canary Islands, Spain) began a violent eruption that lasted about three months. Lava flows and tephra were ejected discontinuously from the volcano. The ashfall deposited over most of the island during the eruptive episode (19/09/2021–13/12/2021) contains, in addition to the usual constituents of volcanic tephra (e.g. volcanic glass, silicates such as olivine, amphibole or pyroxene, magnetite, etc.), a significant amount of very fine-grained (diameter range of 10–500 μm) crystals of highly soluble salts such as AlF_3, NaCl, KCl and $CaSO_4$ (Sánchez-España et al., 2023).

The evolution of Fe speciation and concentration was followed along the coast of La Palma during the eruption of the Tajogaite volcano. The eruption started on 19 September 2021, 7 km from the coast, at the Cabeza de Vaca site. This was considered as Day 0 in this study. The eruption took place near several towns, so topographic models were made to calculate where lava flows could potentially reach the coast. On 22 and 23 September, three stations were sampled at the three possible locations (at the north, centre, and south) where the lava could arrive. The three stations were ~4 km apart. The original sampling sites were covered by lava on 28 September, 10 November, and 22 November.

Sampling was performed during the whole eruptive phase and the two following months in the post-eruptive phase. The sea surface temperature in the non-influenced region averaged ~25 °C in September to ~21 °C in January. During the eruptive phase, the arrival of lava into the seawater produced increases in seawater temperature. The highest recorded temperature was 46.33 °C on November 12, about 10 m away from the frontal lava zone. These increases in seawater temperature were related to the heat transfer between the incandescent lava and the seawater (González-Santana et al., 2022).

During the eruptive phase, heat transfer between lava and the seawater formed thin and shallow hydrothermal plumes (González-Santana et al., 2022). These plumes were characterised by the formation of buoyant plumes next to the lava-sea interface, which were transported adjacent to the sea surface for >1.5 km from the coast. The plume depth was <1 m at distances of 300–500 m from the coast. The plume was characterised by low pH, high pCO_2, high seawater temperatures, and increases in turbidity that could be tracked by the eye (González-Santana et al., 2022). Sampling was always performed at 30 cm depth.

No seawater trace metal measurements are available of the study area before the beginning of the eruption. Initial Fe concentrations measured before the arrival of lava in the region were considered background concentrations. However, this does not imply that Fe from ash could be contributing to the measured concentration. This hypothesis is based on the fact that all samples analysed after this date showed higher Fe concentrations for all size fractions. The initial TdFe, dFe and sFe concentrations were 82.0 ± 31.3, 6.94 ± 2.18 and 0.57 ± 0.20 nM (n = 6) respectively.

In the open surface waters of the Atlantic Ocean, dFe concentrations range from 0.1 to 0.8 nM (Boye et al., 2006; Rijkenberg et al., 2008). Iron concentrations vary depending on the area studied as a result of changes in sources, mesoscale processes and primary production. In Macaronesia, the dFe concentration ranges from 0.46 to 1.32 nM (mean 0.80 ± 0.25 nM). In the Canary Islands, the mean dFe concentration is 0.80 ± 0.16 nM (Arnone et al., 2022).

Initial Fe concentrations (day 5) are 1–2 orders of magnitude higher than those observed in open ocean samples in the North Atlantic, away from hydrothermal systems (Tagliabue et al., 2017). The high concentrations were a result of the sampling location (Arnone et al., 2022). Samples were collected at the surface, 20 m from the shore, where the seafloor depth ranges from 12 to 26 m. The shore was originally volcanic, which, combined with local currents, allowed sediment resuspension and increased particulate loading. Moreover, there could potentially be some Fe arriving to the ocean through volcanic ash

deposition from the initial stages of the eruption before the lava arrived at the ocean. These processes favoured the presence of high Fe concentrations compared to open ocean waters.

At each sampling date, samples were collected around the newly formed volcanic deltas, at approximately the same location considering the growth and erosion of the deltas, the sea conditions and the volcanic activity.

3.1. Temporal evolution of the iron size fractionation

The iron size fractionation was divided into total dissolvable iron (TdFe; unfiltered sample), dissolved iron (dFe, filtered through 0.2 μm), colloidal iron (cFe = dFe - sFe), and soluble iron (sFe, filtered through 0.02 μm) along the La Palma coast during the Tajogaite eruption. Fe concentrations presented high spatial and temporal variability (Fig. 2).

The TdFe concentrations ranged from 33 to 2114 nM (Fig. 2A). These concentrations were strongly influenced by the evolution of the lava's arrival to the seawater. Pre-lava-arrival and post-eruptive samples showed the lowest concentrations, averaging 76 ± 29 nM, n = 12. In contrast, the highest concentrations were observed 5 m from the lava-sea interface, when incandescent lava was observed to be forming laze plumes (2008 ± 75 nM on October 1, 2114 ± 41 nM on November 12 and 2008 ± 49 nM on November 14).

The dFe concentrations reached 69.3 ± 3.0 nM on Day 55 (Fig. 2B). This sample was collected close to the coastline within the plume formed in a highly active event during the formation of a new lava delta. Samplings on November 8 (Day 49) through November 14 (day 55) were performed in a matter of a week which included the formation of a new delta due to a new arrival of lava to the ocean. When comparing days 49 and 55, before and during the formation of a delta and not taking into account the sample within the plume, we observe that both periods presented similar dFe concentrations 28.8 ± 6.1 (n = 6) and 28.6 ± 6.8 nM (n = 6), respectively. Therefore, the high average concentrations observed in day 55 should not be completely related to the formation of the new delta. Some sources of dFe that should be considered during these volcanic events are atmospheric ash deposition and resuspension of fine sediments close to the coastline (Rogan et al., 2016; Sánchez-España et al., 2023).

Soluble Fe concentrations followed a distinct pattern compared to bigger size fractions (TdFe and colloidal particles in dFe, Fig. 2D). The lowest concentrations were measured during the initial outings. Sometime between day 33 and day 49, sFe increased, reaching 17.9 ± 0.1 nM the 12 November. The highest concentrations were measured after day 53 which also coincided with the sampling day with the highest temperature anomaly. Moreover, sFe concentrations remained high on day 61, averaging 7.9 ± 0.9 nM (n = 6) which is one order of magnitude higher than the average dFe concentrations within open ocean waters.

The temporal evolution of Fe during the eruption shows a dynamic environment. Furthermore, sampling dates with high Fe concentrations in all size fractions still contain some samples with low concentrations, in some cases reaching background levels. This presents a mesoscale environment where an area can be strongly affected by the lava-seawater interaction while <1 km away, seawater conditions present non-affected conditions. Submesoscale parametrization should be used in future coastal models presenting this Fe source to the marine environment.

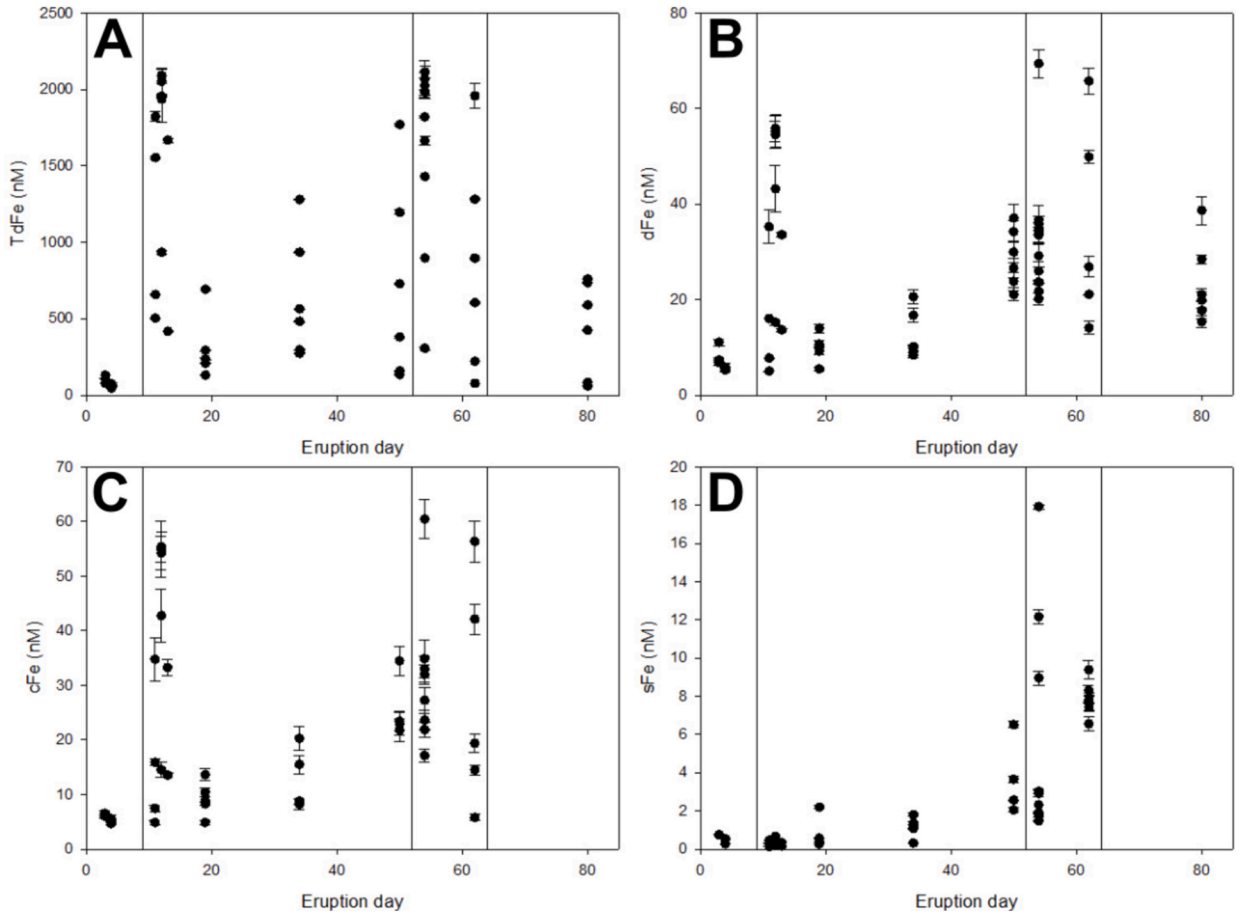

Fig. 2. Temporal evolution of (A) total dissolvable iron (TdFe), (B) dissolved iron (dFe), (C) colloidal iron (cFe = dFe - sFe), and (D) soluble iron (sFe) concentrations along the La Palma coast during the Tajogaite eruption. Day 0 corresponds to September 19, 2021. Black vertical lines correspond to the days new deltas started to form (September 28 (day 8), November 10 (day 51), and November 22, 2021 (day 63)).

3.2. Spatial evolution of the iron size fractionation speciation

Sampling during the volcanic event in ever changing coastal conditions did not allow for repetitive sampling in the same exact sites. Sampling was performed in a ±10 m^2 location. On the one hand, maritime conditions influenced the viability of arriving close to the coast in a safe way, on the other hand, an ongoing eruption presents inherent safety risks, which were always considered and minimized. Moreover, the ongoing eruption drastically changed the coastline in the island, with continuous erosion of new volcanic material.

Fig. 3 presents a combination of the spatial and temporal evolution of the Fe size fractions. Overall, the highest concentrations were observed at the stations closest to the coastline. Exceptions were found at certain dates, where high dFe and TdFe concentrations were also measured 1.5 km from the coast. These results were observed on days when incandescent lava was reaching the seawater (day 53, November 12). The high lava-seafloor activity produced shallow hydrothermal plumes that could be observed from land and sea (González-Santana et al., 2022). The plumes exhibited high turbidity (from 5.5 FTU at 500 m to 1.5 FTU at 1000 m and 0.05 FTU at 1500 m), temperatures (from 36 °C at 500 m to 30 °C at 1000 m and 22 °C at 1500 m) and low pH (from 7.5 at 500 m to 7.7 at 1000 m and 8.0 at 1500 m). These plumes were observed to form near the coast during the active days, to rise rapidly to the surface waters and to disperse similarly to an upwelling filament, at depths ranging from the surface to 10 m depth at the formation site to the surface to 1 m depth, 1.5 km from the coast (González-Santana et al., 2022).

Figs. 3A, B and C present high concentration hotspots just after when the lava arrived in the ocean, September 28 (day 8), November 10 (day 51), and November 22, 2021 (day 63). An interesting characteristic observed from this figure is the latitudinal distribution of the concentration. After the first event on September 28, TdFe dFe and cFe presented a wide spread increase in concentration. However, during the second and third events, the emission points were more localised. The second event occurred towards the south and is observable in panel A as a local maximum in day 51.

3.3. sFe/dFe and dFe/TdFe ratios

The temporal relationship of sFe/dFe and dFe/TdFe was plotted to observe possible interactions between size fractions (Fig. 4). The average trends of all data points show weak to moderate (r: 0.557 and 0.365 and p-value: <0.0001 and <0.005 respectively) increasing percentages of both sFe/dFe and dFe/TdFe with time. The results for dFe/TdFe can be divided into two behaviours. Low percentages were observed before November 8th (day 49; n = 22) as shown in the previous section (Fig. 2). After day 55, the samples showed two different patterns. On the one hand, they presented percentages below 10 %. These samples were collected towards the southern stations, close to where the lava first reached the ocean. On the other hand, the northern stations showed elevated dFe/TdFe ratios. These ratios were predominantly caused by decreasing TdFe concentrations at these stations and supported by dFe concentrations remaining high.

In Fig. 4B the sFe/dFe percentage is depicted. Before day 60, the percentage remained low, below 10 %. The dFe pool was mainly formed by cFe. This period was characterised by the continuous input of ash from the ongoing eruption, which should have acted as a main source of colloidal sized particles.

These results are consistent with the reversible exchange hypothesis between the dFe and pFe presented by Fitzsimmons et al. (2017) and later modelled by González-Santana et al. (2020) and between sFe and cFe by Lough et al. (2019) in deep ocean hydrothermal plumes. However, samples collected during or immediately after strong lava-seawater interactions (black lines in Fig. 2) show lower percentages of sFe/dFe and dFe/TdFe, despite higher sFe and dFe concentrations. This results in a temporal distribution compared to the spatial distribution described in the previous articles. However, the results corroborate each other, where the plume distance is proportional to the time required from its emission from the vent to the location in the water column. Thus, in this coastal regime with high particulate iron loading due to ash deposition, sediment resuspension and lava influx, the flux of iron size fractionation depends on the balance between organic and inorganic stabilisation and the reversibility of exchange to particles (Fig. 5).

There are three main explanations for the increase in large-sized Fe concentrations. Firstly, there may be a decrease in the amount of Fe sourced as soluble iron and smaller particles compared to larger size fractions, such as ash deposition (González-Santana et al., 2020; Rogan et al., 2016). Secondly, there may be aggregation processes occurring, including coagulation, agglomeration and adsorption (Fang and Wang, 2021; Fitzsimmons et al., 2014; González-Santana et al., 2020; Rogan

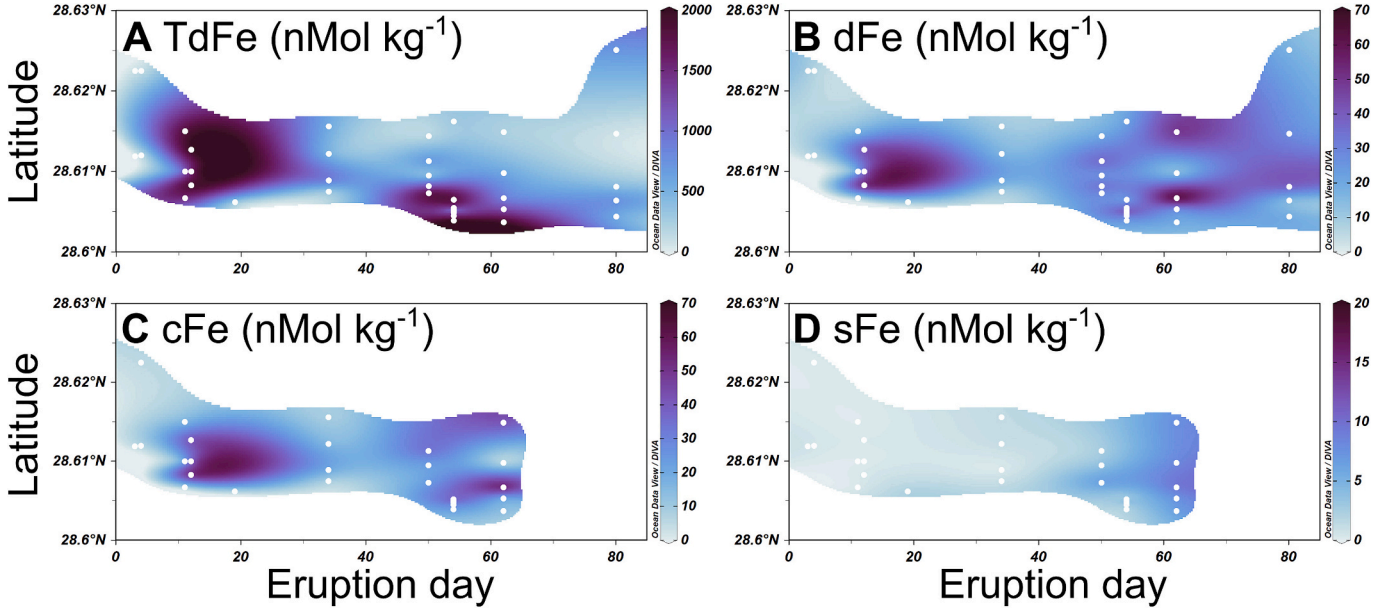

Fig. 3. Spatial evolution of (A) TdFe, (B) dFe and (C) cFe and (D) sFe from samples collected 5–15 m from the La Palma coastline during the eruption. Day 0 corresponds to September 19, 2021.

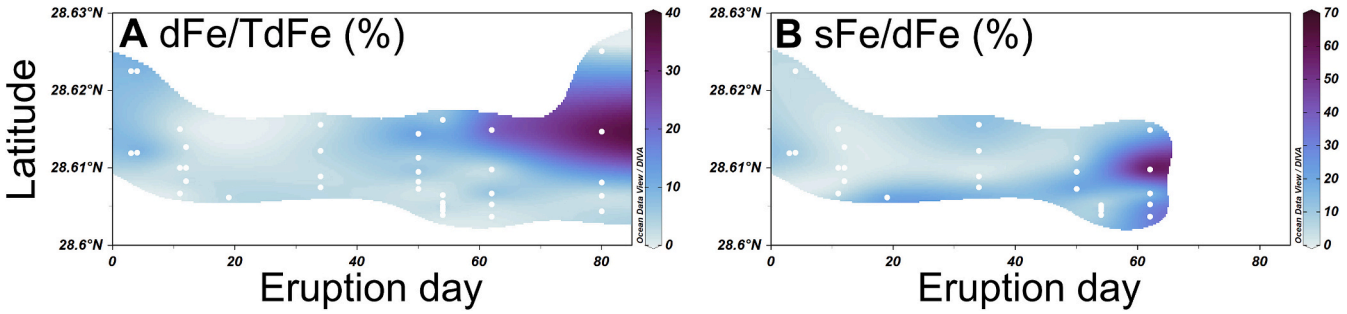

Fig. 4. Spatial and temporal evolution of percentages of A) dFe/TdFe and B) sFe/dFe, percentages reach 40 and 70 % respectively. Day 0 corresponds to September 19, 2021.

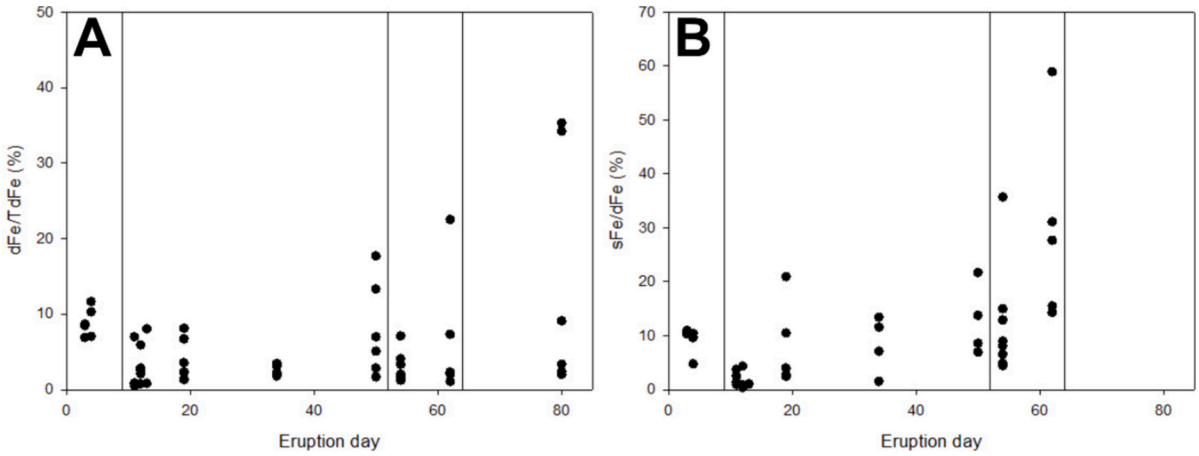

Fig. 5. Temporal evolution of (A) the percentage of dissolved iron content within the readily available iron (dFe/TdFe) and (B) the percentage of soluble content within the dissolved phase (dFe/TdFe). Day 0 corresponds to September 19, 2021.

et al., 2016). This phenomenon has previously been observed in trace metal samples extracted from deep ocean hydrothermal vents, where particles of colloidal size can cause the clogging of 0.45 μm pore size filters (González-Santana et al., 2020). And thirdly, it could be caused by dry deposition, were a relatively greater source of volcanic ash (>0.2 μm) compared to sources of dFe would affect the dFe/TdFe ratio (Rogan et al., 2016). This deposition will be also affected not only by the amount and size ejected by the volcano but also by the predominant wind stress and direction over the affected area.

The size fractionation distribution should also be affected by the physico-chemical properties of the seawater during the eruption. Studies that examine the relationship between reaction temperature and the properties of nanoparticles, demonstrate that higher reaction temperatures lead to an increase in the average size of nanoparticles (Qu et al., 2006). Furthermore, the magnetic properties of nanoparticles are highly dependent on particle size. This makes hydrothermally influenced seawater conditions ideal for iron oxide aggregation processes where compounds such as Fe_3O_4, $MnFe_2O_4$ and $CoFe_2O_4$ are present.

Trace metal residence times presented by previous authors (Bruland et al., 1994; Croot et al., 2004; González-Santana et al., 2020; Martin and Knauer, 1980; Sarthou et al., 2003) show shorter residence times in samples collected at shallow depths when compared to the deep ocean. Furthermore, Sarthou et al. (2003) describe that shortest residence times are associated with high dust fluxes in surface waters. During the eruption, the high particle load within the top layers of the seawater allowed for possible aggregation processes which could lead to the sinking of the different iron size fractions including those not in the particulate phase (Fang and Wang, 2021). The continuous precipitation of ash from the Tajogaite volcano would have acted similar to dust deposition reducing the residence time of iron within the surface waters. If we combine other processes such as aggregation due to the ash's magnetic properties, Fe residence times would have been reduced to periods of 2 to 5 days, within the shortest periods reported by previously mentioned authors.

The North Atlantic Ocean is characterised by the presence of oligotrophic waters. Here, the main source of Fe comes from atmospheric deposition. Between 71 and 87 % of surface dFe comes from Saharan dust aeolian deposition (Conway and John, 2014). This dust is characterised by low Fe solubility ~1.7 % (Baker et al., 2006)and previous work has shown the concentration of dFe increase by 0.05–0.10 nM after a dust event (Rijkenberg et al., 2008, 2012).

During the Tajogaite eruption, vast amounts of ash fell into the ocean. Sánchez-España et al. (2023) stated that the 10 analysed samples presented "a very homogeneous composition, with very minor to negligible difference between samples as regards to the concentration of major oxides." In their samples, the ash presented an iron (Fe_2O_3) composition ranging between 12 and 14 wt%. Iron within ashfall samples displayed concentrations of 5000 μg Fe/kg ash in most cases, with a few samples displaying peak concentrations comprised between 10,000 and 25,000 μg Fe/kg ash. In an oceanographic context, volcanic ash is within the particulate phase and if completely dissolved would appear in the TdFe samples. Since all the Fe of ash would not be completely dissolved, the following calculations present the lowest limits in ash deposition required to cause the observed increases in Fe. Considering an average Fe concentration in volcanic ash of 5000 μg/kg of ash, and a maximum measured concentration of TdFe reaching 2114 nM (~118 μg/L of seawater) it would require the complete dissolution of ~24 g of ash in 1 L of seawater. During sampling, at least 1 L of seawater was filtered. Although filters got black from volcanic ash, in no filters were we able to observe 24 g of ash. Even if the ash had a peak concentration

of 25,000 μg/kg, it would still require a 5 mm thick layer in our filter (using average collected ash from the volcano). Isopach maps developed for the eruption (Bonadonna et al., 2022) present ash thickness of up to 5 cm in the sampling area. However, this thickness is a result of the whole eruption and not in a short time frame as would be expected in our samples due to particle precipitation.

Our results shows that even though ash may have a much larger aerial dispersion range, the arrival of lava into the ocean which acidifies and heats the seawater has a stronger impact that should be considered when developing iron models in hydrothermal and coastal environments. The strength of this Fe source is highly variable (Fig. 3) depending on the sampling site, sea conditions, and the lava composition which should lead to high variability/error of estimate when developing coastal models. Modelling of this volcanic source (ash and lava) will strongly affect coastal fertilization calculations and the variability in different effects observed in primary production in iron-limited regions.

4. Conclusions

Hot spot emissions in the Canary Archipelago represent short-term emissions of volcanic material. In the most recent eruption, described in this article, the eruption took place on land and some of the lava flows reached the ocean. Concurrently, atmospheric deposition took place. Ash deposition reached the ocean and the study area during most of the sampling period. Both events significantly increased the iron concentration in the seawater. It is found that the increase in Fe concentration depends on the size fractionation of iron. The initial input is mainly in the particulate form with an increase in the colloidal size fraction within the dissolved size fraction. Nevertheless, the soluble iron size fractions increase in seawater, especially when considering a longer time frame where reverse scavenging and disaggregation processes (i.e. dissolution, desorption, etc.) take place. The results show that although there was continuous ash deposition during the eruption, the dominant iron source was located in the lava-seawater interface during short events as a result of new lava flows reaching the ocean. In these events iron was mainly sourced in bigger size fractions. Over 99 % of iron was found in the particulate phase, 0.7 % as colloidal Fe and a 0.03 % as soluble iron. Measured dissolved Fe concentrations were up to 18 times higher than the average Canary Islands' concentration. These results highlight the significant role of volcanic activity in influencing iron distribution in coastal environments, particularly through episodic interactions between lava and seawater.

CRediT authorship contribution statement

David González-Santana: Writing – review & editing, Writing – original draft, Visualization, Investigation, Formal analysis, Conceptualization. **Melchor González-Dávila:** Writing – review & editing, Writing – original draft, Visualization, Supervision, Methodology, Investigation, Funding acquisition, Conceptualization. **Aridane G. González:** Writing – review & editing, Visualization, Validation, Supervision, Investigation. **Alfonso Medina-Escuela:** Writing – review & editing, Software, Resources, Methodology. **David Fariña:** Writing – review & editing, Software, Resources, Methodology. **J. Magdalena Santana-Casiano:** Writing – review & editing, Visualization, Supervision, Project administration, Methodology, Investigation, Funding acquisition, Conceptualization.

Declaration of competing interest

The authors declare that they have no known competing financial interests or personal relationships that could have appeared to influence the work reported in this paper.

Acknowledgements

This work was financially supported by the FeRIA project, Fe Response In an Acidified ocean, (PID2021-123997NB-I00) from the Ministerio de Ciencia e Innovación (Spain).

We would like to thank the Canary Islands Emergency Volcanic Plan (PEVOLCA) and its director (Miguel Ángel Morcuende) for the facilities provided for this study. We also thank the Salvamento Maritimo en Canarias and the Salvamar Alphard crew for the means provided for the study. Special thanks go to the Spanish Guardia Civil, its marine group, and GEAS for their effort and dedication, providing us with two ships and crew, the "Pico Teide" and zodiac for sampling and ROV work, particularly to Captain Roberto Duran González for providing all the necessary resources. Thanks also to the Capitanía Marítima de Santa Cruz de Tenerife and the Regional and National Governments for the permission for sampling inside the exclusion zone. We would like also to thank Estudios Ambientales y Oceanografía (ECOS) for providing the AAQ multiparametric sensor. This research is part of the activities of the Observatorio Marino de Cambio Climático (OMACC) del Faro de Fuencaliente de La Palma.

Data availability

Data will be made available on request.

References

Arnone, V., González-Santana, D., González-Dávila, M., González, A.G., Santana-Casiano, J.M., 2022. Iron and copper complexation in Macaronesian coastal waters. Mar. Chem. 240, 104087. https://doi.org/10.1016/J.MARCHEM.2022.104087.

Baker, A.R., Jickells, T.D., Witt, M., Linge, K.L., 2006. Trends in the solubility of iron, aluminium, manganese and phosphorus in aerosol collected over the Atlantic Ocean. Mar. Chem. 98, 43–58. https://doi.org/10.1016/j.marchem.2005.06.004.

Bonadonna, C., Pistolesi, M., Biass, S., Voloschina, M., Romero, J., Coppola, D., Folch, A., D'Auria, L., Martin-Lorenzo, A., Dominguez, L., Pastore, C., Reyes Hardy, M., Rodríguez, F., 2022. Physical characterization of long-lasting hybrid eruptions: the 2021 Tajogaite eruption of Cumbre Vieja (La Palma, Canary Islands). J. Geophys. Res. Solid Earth 127. https://doi.org/10.1029/2022JB025302.

Boye, M., Aldrich, A., van den Berg, C.M.G., de Jong, J.T.M., Nirmaier, H., Veldhuis, M.J. W., Timmermans, K.R., de Baar, H.J.W., 2006. The chemical speciation of iron in the north-east Atlantic Ocean. Deep Sea Res. I Oceanogr. Res. Pap. 53, 667–683. https://doi.org/10.1016/j.dsr.2005.12.015.

Breitbarth, E., Achterberg, E.P., Ardelan, M.V., Baker, A.R., Bucciarelli, E., Chever, F., Croot, P.L., Duggen, S., Gledhill, M., Hassellöv, M., Hassler, C.S., Hoffmann, L.J., Hunter, K.A., Hutchins, D.A., Ingri, J., Jickells, T.D., Lohan, M.C., Nielsdóttir, M.C., Sarthou, G., Schoemann, V., Trapp, J.M., Turner, D.R., Ye, Y., 2010. Iron biogeochemistry across marine systems - progress from the past decade. Biogeosciences 7, 1075–1097. https://doi.org/10.5194/bg-7-1075-2010.

Bruland, K.W., Lohan, M.C., 2006. Controls of trace metals in seawater. In: The Oceans and Marine Geochemistry, vol. 6, pp. 23–47.

Bruland, K.W., Orians, K.J., Cowen, J.P., 1994. Reactive trace metals in the stratified central North Pacific. Geochim. Cosmochim. Acta 58, 3171–3182. https://doi.org/10.1016/0016-7037(94)90044-2.

Conway, T.J., John, S.G., 2014. Quantification of dissolved iron sources to the North Atlantic Ocean. Nature 511, 212–215. https://doi.org/10.1038/nature13482.

Croot, P.L., Streu, P., Baker, A.R., 2004. Short residence time for iron in surface seawater impacted by atmospheric dry deposition from Saharan dust events. Geophys. Res. Lett. 31. https://doi.org/10.1029/2004GL020153.

Cutter, G.A., Casciotti, K., Croot, P., Geibert, W., Heimbürger, L.-E., Lohan, M.C., Planquette, H., van de Flierdt, T., 2017. Sampling and Sample-handling Protocols for GEOTRACES Cruises, Version 3.0.

De Ronde, C.E.J., Baker, E.T., Massoth, G.J., Lupton, J.E., Wright, I.C., Sparks, R.J., Bannister, S.C., Reyners, M.E., Walker, S.L., Greene, R.R., Ishibashi, J., Faure, K., Resing, J.A., Lebon, G.T., 2007a. Submarine hydrothermal activity along the mid-Kermadec Arc, New Zealand: large-scale effects on venting. Geochem. Geophys. Geosyst. 8. https://doi.org/10.1029/2006GC001495.

De Ronde, C.E.J., Baker, E.T., Massoth, G.J., Lupton, J.E., Wright, I.C., Sparks, R.J., Bannister, S.C., Reyners, M.E., Walker, S.L., Greene, R.R., Ishibashi, J., Faure, K., Resing, J.A., Lebon, G.T., 2007b. Submarine hydrothermal activity along the mid-Kermadec Arc, New Zealand: large-scale effects on venting. Geochem. Geophys. Geosyst. 8. https://doi.org/10.1029/2006GC001495.

Delmelle, P., Lambert, M., Dufrêne, Y., Gerin, P., Óskarsson, N., 2007. Gas/aerosol–ash interaction in volcanic plumes: new insights from surface analyses of fine ash particles. Earth Planet. Sci. Lett. 259, 159–170. https://doi.org/10.1016/j.epsl.2007.04.052.

Duggen, S., Croot, P.L., Schacht, U., Hoffmann, L.J., 2007. Subduction zone volcanic ash can fertilize the surface ocean and stimulate phytoplankton growth: evidence from

biogeochemical experiments and satellite data. Geophys. Res. Lett. 34. https://doi.org/10.1029/2006GL027522.
Duggen, S., Olgun, N., Croot, P.L., Hoffmann, L.J., Dietze, H., Delmelle, P., Teschner, C., Skolen, A.P.M., 2010. The role of airborne volcanic ash for the surface ocean biogeochemical iron-cycle: a review. Biogeosciences 7, 827–844.
El-Desoky, A., Hassan, A., Mahmoud, A., 2018. Volcanic ash as a material for soil conditioner and fertility. J. Soil Sci. Agric. Eng. 9, 491–495. https://doi.org/10.21608/JSSAE.2018.36445.
Fang, Z., Wang, W.-X., 2021. Size speciation of dissolved trace metals in hydrothermal plumes on the Southwest Indian Ridge. Sci. Total Environ. 771, 145367. https://doi.org/10.1016/j.scitotenv.2021.145367.
Fisher, R.V., Schmincke, H.-U., 1984. Volcanoes, volcanic rocks and magma chambers. In: Fisher, R.V., Schmincke, H.-U. (Eds.), Pyroclastic Rocks. Springer Berlin Heidelberg, Berlin, Heidelberg, pp. 11–34. https://doi.org/10.1007/978-3-642-74864-6_2.
Fitzsimmons, J.N., Boyle, E.A., Jenkins, W.J., 2014. Distal transport of dissolved hydrothermal iron in the deep South Pacific Ocean. Proc. Natl. Acad. Sci. 111. https://doi.org/10.1073/pnas.1418778111, 16654 LP–16661.
Fitzsimmons, J.N., John, S.G., Marsay, C.M., Hoffman, C.L., Nicholas, S.L., Toner, B.M., German, C.R., Sherrell, R.M., 2017. Iron persistence in a distal hydrothermal plume supported by dissolved-particulate exchange. Nat. Geosci. 10, 195–201. https://doi.org/10.1038/ngeo2900.
Frogner, P., Reynir Gíslason, S., Óskarsson, N., 2001. Fertilizing potential of volcanic ash in ocean surface water. Geology 29, 487. https://doi.org/10.1130/0091-7613(2001)029<0487:FPOVAI>2.0.CO;2.
Galetto, F., Pritchard, M.E., Hornby, A.J., Gazel, E., Mahowald, N.M., 2023. Spatial and temporal quantification of subaerial volcanism from 1980 to 2019: solid products, masses, and average eruptive rates. Rev. Geophys. 61, e2022RG000783. https://doi.org/10.1029/2022RG000783.
Gíslason, S.R., Snorrason, Á., Kristmannsdóttir, H.K., Sveinbjörnsdóttir, Á.E., Torsander, P., Ólafsson, J., Castet, S., Dupré, B., 2002. Effects of volcanic eruptions on the CO_2 content of the atmosphere and the oceans: the 1996 eruption and flood within the Vatnajökull Glacier, Iceland. Chem. Geol. 190, 181–205. https://doi.org/10.1016/S0009-2541(02)00116-X.
González-Delgado, S., González-Santana, D., Santana-Casiano, J.M., González-Dávila, M., Hernández, C.A., Sangil, C., Hernández, J.C., 2021. Chemical characterization of the Punta de Fuencaliente CO_2-enriched system (La Palma, NE Atlantic Ocean): a new natural laboratory for ocean acidification studies. Biogeosciences 18, 1673–1687. https://doi.org/10.5194/BG-18-1673-2021.
González-Santana, D., Planquette, H., Cheize, M., Whitby, H., Gourain, A., Holmes, T.M., Guyader, V., Cathalot, C., Pelleter, E., Fouquet, Y., Sarthou, G., 2020. Processes driving iron and manganese dispersal from the TAG hydrothermal plume (mid-Atlantic ridge): results from a GEOTRACES process study. Front. Mar. Sci. 7, 568. https://doi.org/10.3389/fmars.2020.00568.
González-Santana, D., Santana-Casiano, J.M., González, A.G., González-Dávila, M., 2022. Coastal carbonate system variability along an active lava–seawater interface. Front. Mar. Sci. 9. https://doi.org/10.3389/fmars.2022.952203.
Hawco, N.J., Yang, S.C., Foreman, R.K., Funkey, C.P., Dugenne, M., White, A.E., Wilson, S.T., Kelly, R.L., Bian, X., Huang, K.F., Karl, D.M., John, S.G., 2020. Metal isotope signatures from lava-seawater interaction during the 2018 eruption of Kīlauea. Geochim. Cosmochim. Acta 282, 340–356. https://doi.org/10.1016/J.GCA.2020.05.005.
Kelly, L.J., Fauria, K.E., Mittal, T., El Kassar, J., Bennartz, R., Nicholson, D., Subramaniam, A., Gupta, A.K., 2023. Ash deposition triggers phytoplankton blooms at Nishinoshima volcano, Japan. Geochem. Geophys. Geosyst. 24, e2023GC010914. https://doi.org/10.1029/2023GC010914.
Lohan, M.C., Aguilar-Islas, A.M., Bruland, K.W., 2006. Direct determination of iron in acidified (pH 1.7) seawater samples by flow injection analysis with catalytic spectrophotometric detection: application and intercomparison. Limnol. Oceanogr. Methods 4 (6), 164–171. https://doi.org/10.4319/lom.2006.4.164.
Lough, A.J.M., Homoky, W.B., Connelly, D.P., Comer-Warner, S.A., Nakamura, K., Abyaneh, M.K., Kaulich, B., Mills, R.A., 2019. Soluble iron conservation and colloidal iron dynamics in a hydrothermal plume. Chem. Geol. 511, 225–237.
Martin, J.H., Knauer, G.A., 1980. Manganese cycling in northeast Pacific waters. Earth Planet. Sci. Lett. 51, 266–274. https://doi.org/10.1016/0012-821X(80)90209-5.
Mason, E., Wieser, P.E., Liu, E.J., Edmonds, M., Ilyinskaya, E., Whitty, R.C.W., Mather, T. A., Elias, T., Nadeau, P.A., Wilkes, T.C., McGonigle, A.J.S., Pering, T.D., Mims, F.M., Kern, C., Schneider, D.J., Oppenheimer, C., 2021. Volatile metal emissions from volcanic degassing and lava–seawater interactions at Kīlauea Volcano, Hawai'i. Commun. Earth Environ. 2, 1–16. https://doi.org/10.1038/s43247-021-00145-3.
Maters, E.C., Delmelle, P., Bonneville, S., 2016. Atmospheric processing of volcanic glass: effects on Iron solubility and redox speciation. Environ. Sci. Technol. 50, 5033–5040. https://doi.org/10.1021/acs.est.5b06281.
Millero, F.J., 1986. The pH of estuarine waters. Limnol. Oceanogr. 31, 839–847. https://doi.org/10.4319/lo.1986.31.4.0839.
Nakagawa, M., Ohba, T., 2002. Minerals in volcanic ash 1: primary minerals and volcanic glass. Glob. Environ. Res.-English Edition 6, 41–52.
Naughton, J.J., Greenberg, V.A., Goguel, R., 1976. Incrustations and fumarolic condensates at Kilauea volcano, Hawaii: field, drill-hole and laboratory observations. J. Volcanol. Geotherm. Res. 1, 149–165. https://doi.org/10.1016/0377-0273(76)90004-4.
Obata, H., Karatani, H., Nakayama, E., 1993. Automated determination of iron in seawater by chelating resin concentration and chemiluminescence detection. Anal. Chem. 65, 1524–1528. https://doi.org/10.1021/ac00059a007.
Olafsson, J., 1975. Volcanic influence on seawater at Heimaey. Nature 255, 138–141. https://doi.org/10.1038/255138a0.
Olgun, N., Duggen, S., Croot, P.L., Delmelle, P., Dietze, H., Schacht, U., Óskarsson, N., Siebe, C., Auer, A., Garbe-Schönberg, D., 2011. Surface ocean iron fertilization: the role of airborne volcanic ash from subduction zone and hot spot volcanoes and related iron fluxes into the Pacific Ocean. Glob. Biogeochem. Cycles 25. https://doi.org/10.1029/2009GB003761.
Óskarsson, N., 1981. The chemistry of icelandic lava incrustations and the latest stages of degassing. J. Volcanol. Geotherm. Res. 10, 93–111. https://doi.org/10.1016/0377-0273(81)90057-3.
Qu, Y., Yang, H., Yang, N., Fan, Y., Zhu, H., Zou, G., 2006. The effect of reaction temperature on the particle size, structure and magnetic properties of coprecipitated $CoFe_2O_4$ nanoparticles. Mater. Lett. 60, 3548–3552. https://doi.org/10.1016/j.matlet.2006.03.055.
REDMIC, 2022. Repositorio de Datos Marinos Integrados de Canarias [WWW Document]. URL. https://en.redmic.es/atlas. (Accessed 26 March 2022).
Resing, J.A., Sansone, F.J., 1999. The chemistry of lava–seawater interactions: the generation of acidity. Geochim. Cosmochim. Acta 63, 2183–2198. https://doi.org/10.1016/S0016-7037(99)00193-3.
Resing, J.A., Sansone, F.J., 2002. The chemistry of lava-seawater interactions II: the elemental signature. Geochim. Cosmochim. Acta 66, 1925–1941. https://doi.org/10.1016/S0016-7037(01)00897-3.
Rijkenberg, M.J.A., Powell, C.F., Dall'Osto, M., Nielsdottir, M.C., Patey, M.D., Hill, P.G., Baker, A.R., Jickells, T.D., Harrison, R.M., Achterberg, E.P., 2008. Changes in iron speciation following a Saharan dust event in the tropical North Atlantic Ocean. Mar. Chem. 110, 56–67. https://doi.org/10.1016/j.marchem.2008.02.006.
Rijkenberg, M.J.A., Steigenberger, S., Powell, C.F., van Haren, H., Patey, M.D., Baker, A. R., Achterberg, E.P., 2012. Fluxes and distribution of dissolved iron in the eastern (sub-) tropical North Atlantic Ocean. Glob. Biogeochem. Cycles 26. https://doi.org/10.1029/2011GB004264.
Rogan, N., Achterberg, E.P., Le Moigne, F.A.C., Marsay, C.M., Tagliabue, A., Williams, R. G., 2016. Volcanic ash as an oceanic iron source and sink. Geophys. Res. Lett. 43, 2732–2740. https://doi.org/10.1002/2016GL067905.
Sánchez-España, J., Mata, M.P., Vegas, J., Lozano, G., Mediato, J., Martínez Martínez, J., Galindo, I., Sánchez, N., del Moral, B., Ordóñez, B., de Vergara, A., Nieto, A., Andrés, M., Vázquez, I., Bellido, E., Castillo-Carrión, M., 2023. Leaching tests reveal fast aluminum fluoride release from ashfall accumulated in La Palma (Canary Islands, Spain) after the 2021 Tajogaite eruption. J. Volcanol. Geotherm. Res. 444, 107959. https://doi.org/10.1016/j.jvolgeores.2023.107959.
Sansone, F.J., Resing, J.A., 1995. Hydrography and geochemistry of sea surface hydrothermal plumes resulting from Hawaiian coastal volcanism. J. Geophys. Res. Oceans 100, 13555–13569. https://doi.org/10.1029/95JC01120.
Sarthou, G., Baker, A.R., Blain, S., Achterberg, E.P., Boye, M., Bowie, A.R., Croot, P.L., Laan, P., de Baar, H.J.W., Jickells, T.D., Worsfold, P.J., 2003. Atmospheric iron deposition and sea-surface dissolved iron concentrations in the eastern Atlantic Ocean. Deep-Sea Res. I Oceanogr. Res. Pap. 50, 1339–1352. https://doi.org/10.1016/S0967-0637(03)00126-2.
Spirakis, C.S., 1991. Iron fertilization with volcanic ash? EOS Trans. Am. Geophys. Union 72, 525.
Spokes, L.J., Jickells, T.D., 1996. Factors controlling the solubility of aerosol trace metals in the atmosphere and on mixing into seawater. Aquat. Geochem. 1, 355–374. https://doi.org/10.1007/BF00702739.
Strickland, J.D.H., Parsons, T.R., 1972. A Practical Handbook of Seawater Analysis. Fisheries Research Board of Canada, p. 310.
Tagliabue, A., Bowie, A.R., Boyd, P.W., Buck, K.N., Johnson, K.S., Saito, M.A., 2017. The integral role of iron in ocean biogeochemistry. Nature. https://doi.org/10.1038/nature21058.
Watson, A.J., 1997. Volcanic iron, CO_2, ocean productivity and climate. Nature 385, 587–588. https://doi.org/10.1038/385587b0.
Wilson, S.T., Hawco, N.J., Armbrust, E.V., Barone, B., Björkman, K.M., Boysen, A.K., Burgos, M., Burrell, T.J., Casey, J.R., DeLong, E.F., Dugenne, M., Dutkiewicz, S., Dyhrman, S.T., Ferrón, S., Follows, M.J., Foreman, R.K., Funkey, C.P., Harke, M.J., Henke, B.A., Hill, C.N., Hynes, A.M., Ingalls, A.E., Jahn, O., Kelly, R.L., Knapp, A.N., Letelier, R.M., Ribalet, F., Shimabukuro, E.M., Tabata, R.K.S., Turk-Kubo, K.A., White, A.E., Zehr, J.P., John, S.G., Karl, D.M., 2019. Kīlauea lava fuels phytoplankton bloom in the North Pacific Ocean. Science 1979 (365), 1040–1044.